Research Square

Preprints are preliminary reports that have not undergone peer review.
They should not be considered conclusive, used to inform clinical practice,
or referenced by the media as validated information.

Extreme Immune Checkpoint Inhibitor–Associated Thrombocytosis with Concurrent C-MET Upregulation Evolution in Extensive-Stage Small Cell Lung Cancer: A Case Report

Congcong Huang
Hainan Medical University Affiliated Cancer Hospital
Jun Wu
Hainan Medical University Affiliated Cancer Hospital
Xiayu Wu
Hainan Medical University Affiliated Cancer Hospital
Quan Cheng
Hainan Medical University Affiliated Cancer Hospital
Zhao Zhang
m18889786061@muhn.edu.cn

Hainan Medical University Affiliated Cancer Hospital

Case Report

Keywords: Immune checkpoint inhibitors, Thrombocytosis, Small cell lung cancer, Hemophagocytic lymphohistiocytosis, C-MET

Posted Date: September 1st, 2026

DOI: https://doi.org/10.21203/rs.3.rs-10530746/v1

License: This work is licensed under a Creative Commons Attribution 4.0 International License.
Read Full License

Additional Declarations: No competing interests reported.

Abstract

Background.

Extensive-stage small cell lung cancer (ES-SCLC) carries a dismal prognosis. Immune checkpoint inhibitors (ICIs) have modestly improved survival, but durable responses are uncommon, and hematologic immune-related adverse events (irAEs)—<1% of treated patients—remain poorly characterised. Extreme reactive thrombocytosis (> 1,000 × 10^9/L) has not been documented during ICI therapy for ES-SCLC, and its mechanism and management are undefined. Endocrine irAEs (secondary adrenal insufficiency) are increasingly recognised, but their concurrence with hematologic toxicity has not been described.

Case Presentation.

A 62-year-old man with ES-SCLC received first-line Toripalimab-based immunotherapy. On day 71 (24 February 2026), the platelet count peaked at 1,033 × 10^9/L, prompting urgent therapeutic plateletpheresis. Concurrent serology showed interferon-γ approximately 45 times the upper limit of normal (ULN), ferritin approximately 20× ULN, and elevated soluble interleukin-2 receptor, consistent with an incomplete hemophagocytic lymphohistiocytosis (HLH) phenotype. C-reactive protein peaked at 178.40 mg/L and interleukin-6 reached 199.68 pg/mL on 2 March 2026, supporting cytokine-driven myeloproliferation. Serial tumor biopsies documented C-MET evolution from 10% weak-positive to 80% strong-positive. Early tumor shrinkage (11% reduction from a 118-mm baseline) coincided with the platelet peak on day 71, while maximal radiographic response (50% reduction) was achieved on day 121 (15 April 2026). Treatment was modified with antiangiogenic optimization (Anlotinib 12 mg daily) and Toripalimab was substituted with Tislelizumab. Consolidative thoracic radiotherapy (PTV 45 Gy/25 fractions, PGTV 50 Gy/25 fractions, simultaneous integrated boost) commenced on 23 May 2026. On the same day, endocrinology consultation confirmed secondary adrenal insufficiency (ACTH < 0.22 pmol/L, cortisol < 2.76 nmol/L), managed with prednisolone replacement and blood pressure restoration.

Conclusions.

The temporal sequence—peak platelet count (day 71) preceding maximal tumor response (day 121) implicates immune activation, not tumor burden, as the thrombocytosis driver. C-MET upregulation under PD-1 blockade may represent both a resistance mechanism and a targetable salvage pathway. This first reported concurrence of extreme thrombocytosis, incomplete HLH, and secondary adrenal insufficiency in a single ES-SCLC patient underscores the need for multi-system irAE monitoring.

Trial Registration

Clinical trial number: not applicable. This is a retrospective single-patient case report; no prospective clinical trial was conducted, and no patient was enrolled in a registered clinical trial for the treatments described.

1. Introduction

Small cell lung cancer (SCLC) accounts for ~ 13–15% of lung cancers, with rapid progression and poor prognosis. ICIs targeting PD-1/PD-L1 have modestly improved outcomes in extensive-stage disease (ES-SCLC) [19, 20, 21, 22], yet most patients progress within months. ICI therapy induces a spectrum of irAEs [1, 7]. Hematological irAEs—<1% of all irAE reports—are increasingly recognised [2, 5, 8]. ICI-related fatalities, though uncommon, have been documented in a meta-analysis [2].

ITP is the most frequent platelet abnormality [4, 11]; ICI-associated thrombocytosis is exceptionally rare, with extreme values (> 1,000 × 10^9/L) not previously reported. C-MET upregulation is a major mechanism of acquired resistance in SCLC [10, 18], often accompanied by aggressive tumor behavior.

We report a case of ES-SCLC in which Toripalimab-based therapy was associated with extreme reactive thrombocytosis requiring therapeutic plateletpheresis, dramatic C-MET upregulation on serial biopsies, and secondary adrenal insufficiency developing during consolidative radiotherapy. The temporal sequence—peak platelet count (day 71) preceding maximal tumor response (day 121)—offers mechanistic insight into immune-mediated hematologic toxicity. Prepared per CARE 2013/2016 guidelines [24].

2. Case Presentation

The comprehensive clinical course—including sequential treatments, tumor burden trajectory, hematologic dynamics, and inflammatory biomarker evolution—is illustrated in Fig. 1.

2.1 Patient Characteristics

A 62-year-old man (45 kg, BMI 16.0, ECOG 1; 38 pack-years) was admitted to Hainan Cancer Hospital on 24 February 2026 (first admission) for evaluation of a right upper lobe lung mass. Baseline labs were unremarkable except elevated NSE and ProGRP (consistent with SCLC). ^{18}F-FDG PET/CT (21 Nov 2025) showed a hypermetabolic right upper lobe mass (SUVmax 17.0), mediastinal nodal involvement, and a solitary segment-5 hepatic metastasis (23 mm, SUVmax 9.5) (Fig. 1). The clinical diagnosis was right upper lobe malignant neoplasm (small cell lung cancer, extensive-stage).

(See Table 1 for full baseline demographics, clinical characteristics, and diagnostic workup.)

Table 1
Baseline Demographics, Clinical Characteristics, and Diagnostic Workup

Characteristic	Value	Reference / Note
Patient Demographics		
Age, years	62	—
Sex	Male	—
Body mass index, kg/m²	16.0	Cachexia threshold < 18.5
Weight, kg	45	—
ECOG performance status	1	0–5 scale
Smoking history, pack-years	38	Heavy smoker (≥ 30)
Past Medical History		
Prior malignancy / autoimmune disease / chemo-radiotherapy	None	—
Concomitant medications	None reported	—
Presenting History		
Initial clinical encounter (outpatient CT)	2025-11-19	Incidental right upper lobe mass
First admission to our hospital	2026-02-24	Hainan Cancer Hospital
Pathology (Initial Biopsy)		
Biopsy site / date	Right supraclavicular lymph node / 2025-11-21	Pathology report 2025-11-26
Histologic diagnosis	Small cell carcinoma	—
Ki-67 proliferation index	90%+	High-grade neuroendocrine
C-MET (IHC, LBP4 clone)	10%, weak+	Later 80% strong + at re-biopsy (Jan 2026)
Synaptophysin / CD56 / INSM1	All positive	Neuroendocrine marker panel
Chromogranin A	Negative	—
TTF-1	Individual cells positive	—
PD-L1 (IHC, 22C3)	Not tested	Not required for ICI eligibility in SCLC (CSCO guideline)
Disease Staging		

Characteristic	Value	Reference / Note
Clinical stage	Extensive-stage SCLC (ES-SCLC)	VALG / TNM 8th
Primary tumor location / size	Right upper lobe / 81×53 mm	PET/CT 2025-11-21
Primary tumor SUVmax	17.0	^{18}F-FDG PET/CT
Lymph node involvement	Right hilar, mediastinal (4R), right supraclavicular	—
Largest lymph node / SUVmax	64×56 mm / 15.2	Station 4R
Distant metastasis	Solitary hepatic (segment 5, 23 mm, SUVmax 9.5)	—
CNS imaging (MRI)	Not performed	Asymptomatic; no neurological deficit
Bone scan (^{99}Tc-MDP)	Not required	^{18}F-FDG PET/CT provided whole-body skeletal evaluation with no suspicious osseous uptake
Baseline Laboratory Values		Reference range
White blood cell count, ×10^9/L	Not separately reported at baseline	3.5–9.5
Haemoglobin, g/L	145 (2025-12-29)	130–175
Platelet count, ×10^9/L	234 (2025-12-29)	125–350
Neuron-specific enolase, ng/mL	19.56 (2025-12-29)	< 16.5
Pro-gastrin-releasing peptide	Elevated (qualitative)	< 78.62 pg/mL
Ferritin, ng/mL	753.5 (2025-12-15)	≤ 375
Erythrocyte sedimentation rate, mm/h	56.5 (2025-12-15)	0–30
Autoimmune Workup		
ANA / autoantibody panel (12 items)	All negative (2026-02-27)	Excludes autoimmune etiology; performed during HLH workup for differential diagnosis
First-Line Therapy		
Regimen (start date 2025-12-16)	Toripalimab 240 mg d1 + EP (etoposide + carboplatin), q3w	Etoposide dose-reduced for cachexia

Table 1 footnote. Baseline values reflect the pre-treatment window (2025-11-19 to 2025-12-29). Dynamic laboratory and radiographic changes during therapy—including the platelet peak of 1,033×10⁹/L on day 71, the cytokine surge (IFN-γ ~45× ULN, ferritin ~20× ULN, IL-6 199.68 pg/mL), and C-MET clonal evolution to 80% strong-positive—are detailed in the main text and Figure 1. PD-L1 immunohistochemistry was not performed because PD-L1 status does not influence ICI eligibility in extensive-stage SCLC under current CSCO guidelines; immunotherapy was administered regardless. Bone scintigraphy (⁹⁹ᵐTc-MDP) was not required as the baseline ¹⁸F-FDG PET/CT provided whole-body skeletal evaluation with no suspicious osseous uptake.

2.2 First-Line Therapy and Initial Response

The patient received two cycles of first-line therapy beginning 16 December 2025: Toripalimab 240 mg (anti-PD-1) on day 1 plus etoposide 60 mg on days 1–4 plus 80 mg on day 5 and carboplatin 400 mg on day 1 (EP regimen, q3w, with etoposide dose reduced for cachexia [BMI 16.0]) (Fig. 1A), administered intravenously every three weeks. CT on 21 January 2026 showed PD per RECIST 1.1: target lesion + 1.7% (below 20% threshold), but new FDG-avid hepatic lesions appeared. A left brachiocephalic vein thrombus was noted; MDT consultation prompted a second biopsy.

2.3 Second Biopsy and Phenotypic Shift on Repeat Biopsy

IHC comparison between Bx1 (right supraclavicular lymph node, 26 Nov 2025) and Bx2 (right upper lobe mass, 21 Jan 2026) revealed SCLC: CD56+, Syn+, INSM1+, TTF-1+, C-MET 10% weak+, Ki-67 90%+. Bx2 demonstrated HG-NEC transformation with striking C-MET upregulation (80% strong+, 10% weak+), Ki-67 decline to 60%, partial Syn/INSM1 attenuation, and CgA newly acquired [18] (Fig. 3). The full 15-marker IHC panel across both biopsies is shown in Fig. 4; full marker panels are detailed in Supplementary Table S1. Ki-67 decline (90%→60%) likely reflects inter-site spatial heterogeneity, not true biological reduction.

2.4 Second-Line Therapy and Tumor Response

Second-line therapy (Feb 2026, Fig. 1A): Anlotinib 8 mg d1–14 [16] + Toripalimab 240 mg d1 + liposomal irinotecan 86 mg d1 + carboplatin 400 mg d2, q3w. After 2 cycles, CT (24 Feb 2026) showed early tumor shrinkage: lung mass 105×60 mm (11% reduction); lymph nodes 64×56→15 mm; hepatic metastasis 23→13×11 mm (Fig. 1B). Representative CT images at the carinal level demonstrating response are shown in (Fig. 2). By 15 April 2026, lung mass 59×53 mm (50% reduction; RECIST PR), hepatic metastasis 11×9 mm, and the brachiocephalic vein thrombus resolved.

Figure 2. Serial contrast-enhanced axial CT at the carinal level demonstrating radiologic response of the right-lung primary mass to sequential immunochemotherapy plus anlotinib. Three time points are shown in lung-window (top row, a–c) and contrast-enhanced mediastinal-window (bottom row, d–f) reconstructions: (A, D) 21 January 2026 (baseline before second-line therapy, tumor longest diameter 118 mm); (B, E) 24 February 2026 (after two cycles of second-line therapy, 11% early shrinkage); (C, F) 15 April 2026 (continued response, tumor longest diameter 59 mm, 50% reduction; partial response per

RECIST 1.1). All images are at the same anatomical level to allow direct slice-by-slice comparison. Note that the carinal plane shown does not represent the maximum cross-section of the tumor; whole-tumor longest diameters are reported in Fig. 1B.

By the third cycle (7 March 2026), all tumor markers had normalized. NSE mirrored tumor burden: 19.56→412.25 ng/mL (~ 25× ULN at PD)→12.67 ng/mL by 14 April 2026.

2.5 Methods: Radiotherapy Protocol

Consolidative thoracic radiotherapy was delivered per institutional MDT protocol with a simultaneous integrated boost (SIB) technique. GTV encompassed the right lung primary tumor, ipsilateral supraclavicular and mediastinal lymph nodes. CTV was generated by 5-mm GTV expansion plus elective coverage of bilateral supraclavicular, ipsilateral hilar, and mediastinal/hilar lymphatic drainage stations. PTV and PGTV were created by 5-mm expansion of CTV and GTV, respectively, with OAR sparing prioritised. Prescription doses: PTV 45 Gy/25 fractions (1.8 Gy/fraction), PGTV 50 Gy/25 fractions (2.0 Gy/fraction); 5 fractions/week (Monday–Friday) with weekly cone-beam CT. Radiotherapy commenced 23 May 2026, scheduled completion approximately 24 June 2026. Systemic antitumor therapy remained suspended pending liver recovery.

2.6 Development of Extreme Thrombocytosis

On 24 February 2026 (day 71), the platelet count peaked at 1,033 × 10^9/L (reference range: 125–350 × 10^9/L)—among the highest platelet counts reported in the ICI-associated hematological toxicity literature. Maximal tumor response (50% reduction) was subsequently achieved on 15 April 2026 (day 121). The patient was asymptomatic for bleeding or thrombosis. TEG (26 February) showed a hypercoagulable profile (values not reported). Primary thrombocytosis was clinically excluded: JAK2 V617F/CALR/MPL profiles not specifically tested, no splenomegaly, and elevated inflammatory markers supported a reactive process. Hematology was consulted the same day; therapeutic plateletpheresis was initiated given the hypercoagulable TEG profile and known thrombus. Low-molecular-weight heparin (LMWH) was continued for anticoagulation; aspirin was not added as the patient was already on therapeutic-dose LMWH.

2.7 Inflammatory Markers and HLH Workup

Marked systemic inflammation accompanied the clinical course. CRP peaked at 178.40 mg/L on 24 February 2026 (~ 18× ULN). IL-6 peaked at 199.68 pg/mL on 2 March 2026 (Fig. 1D). Serum ferritin rose from 753.5 ng/mL (Dec 2025) to 7,419.4 ng/mL on 7 March 2026 (~ 20× ULN; Fig. 1E). IFN-γ by flow cytometry on 3 March 2026 was 669.54 pg/mL (~ 45× ULN; Fig. 5). sIL-2R was 2,561.59 U/mL on 9 March 2026 and 2,101.04 U/mL on 15 April 2026 (Fig. 5). Hyperferritinemia was partly attributable to tumor-related cachexia (BMI 16.0 kg/m^2) and DILI.

HScore peaked at 124 points [23] (T5, 2026-03-02), corresponding to 9–16% HLH probability (trajectory T1 = 41→T5 in Fig. 5A). The absence of bone marrow biopsy and NK-cell activity data precludes

definitive scoring and likely underestimates true probability. Only three of eight HLH-2004 criteria were met (fever, splenomegaly/hepatomegaly, ferritin ≥ 500 ng/mL; Fig. 5D).

2.8 Diagnostic Considerations

Bone marrow biopsy was deferred given thrombocytosis-related bleeding risk; the cytokine profile guided treatment modifications.

2.9 Treatment Modifications and Current Status

On 3 March 2026, given the peak inflammatory markers and cytokine storm, anlotinib was escalated to 12 mg/d. Toripalimab was switched to Tislelizumab [17] from the third cycle (7 March 2026). 3rd cycle (7 March 2026): Tislelizumab 200 mg + liposomal irinotecan 86 mg + carboplatin 400 mg.

On 13 April 2026, the patient was admitted for evaluation of drug-induced liver injury. Lab (14 Apr 2026): ALT 84 U/L, AST 139 U/L (grade 2), TBA 14.0 μmol/L. Hepatoprotective therapy was initiated. By 20 April 2026, ALT and AST showed partial improvement. Discharged with hepatoprotection and weekly LFT monitoring; antitumor therapy suspended pending liver recovery.

2.10 Endocrine irAE and Adrenal Insufficiency

On 23 May 2026—the day of radiotherapy initiation—endocrinology consultation was triggered by 3 days of progressive anorexia. Adrenal axis evaluation revealed panhypopituitarism-pattern biochemistry: ACTH < 0.22 pmol/L at all timepoints (8 AM, 4 PM, midnight) and cortisol < 2.76 nmol/L at 8 AM and 4 PM (3.34 nmol/L at midnight; reference 160–620 nmol/L). The pattern is consistent with **secondary adrenal insufficiency** of pituitary origin, most plausibly ICI-related hypophysitis. Treatment with prednisolone acetate 10 mg (08:00) + 5 mg (16:00) PO daily was initiated. By 26 May 2026, blood pressure had normalised (BP 100–112/59–72 mmHg from admission 79–106/47–66 mmHg), appetite had recovered, and stress-dose glucocorticoid guidance was provided. This is the fourth irAE phenotype—endocrine—occurring in the same patient, after hematologic, hepatic, and cytokine/HLH-mimic events.

2.11 Follow-up and Outcome

The patient began consolidative thoracic radiotherapy on 23 May 2026 (per Methods: Radiotherapy Protocol), with scheduled completion approximately 24 June 2026. Secondary adrenal insufficiency was diagnosed on the same day and managed with prednisolone replacement (see Endocrine irAE). Radiotherapy and endocrine-replacement therapy continue at the time of manuscript preparation. Antitumor systemic therapy remains temporarily suspended pending liver function recovery. Final tumor response assessment and long-term safety follow-up will be reported in a subsequent update.

3. Discussion

We describe four previously unreported phenomena: (1) extreme reactive thrombocytosis (> 1,000 × 10^9/L) as an irAE in ES-SCLC; (2) therapeutic plateletpheresis for ICI-related thrombocytosis; (3) C-MET

clonal evolution under PD-1 pressure concurrent with a hematologic irAE; and (4) secondary adrenal insufficiency as a fourth irAE phenotype. Platelet peak (day 71) preceding maximal tumor response (day 121) implicates immune activation, not tumor burden, as the thrombocytosis driver. Alternative etiologies were excluded: primary thrombocytosis (no splenomegaly, elevated inflammatory markers), iron deficiency (ferritin 7,419 ng/mL), and chemotherapy effect. The triad of cytokine storm, extreme thrombocytosis, and concurrent tumor shrinkage represents a unique hyperinflammatory irAE phenotype in SCLC.

3.1 Mechanistic Pathways

The IL-6/GM-CSF megakaryocyte axis is the hypothesized mechanism [3, 25]. PD-1/PD-L1 blockade activates effector T cells and macrophages, promoting IL-6 and GM-CSF secretion that drive megakaryocyte proliferation. IL-6 peaked at 199.68 pg/mL on 2 March 2026, concurrent with platelet count decline—reflecting a continuum of immune activation. HGF/C-MET activates JAK/STAT3 [10], promoting further IL-6 transcription. C-MET upregulation (10%→80%) is consistent with MYC-driven subtype evolution [9, 10, 18], representing a resistance mechanism and a targetable salvage pathway.

3.2 Clinical Implications and Treatment Modifications

Therapeutic plateletpheresis for ICI-related thrombocytosis is not previously reported. Decision criteria: PLT 1,033 × 10^9/L, hypercoagulable TEG, concurrent thrombus—ASFA category III. We propose plateletpheresis for PLT > 1,000 × 10^9/L with hypercoagulability or thrombosis as bridge therapy. Tislelizumab substitution (Fc-modified) [17] aimed to attenuate immune activation. C-MET strong expression (80% IHC) suggests MET dependence; selective MET inhibitors (Tepotinib, Capmatinib) require FISH/NGS confirmation per NCCN [12, 13, 14].

3.3 Drug-Induced Liver Injury (DILI)

On 13 April 2026, grade 2 hepatotoxicity developed (ALT 84 U/L, AST 139 U/L, TBA 14.0 μmol/L). The contributions of Toripalimab, platinum, irinotecan, and anlotinib cannot be isolated. Hepatoprotective therapy and antitumor-therapy suspension achieved partial biochemical improvement by 20 April 2026. Routine LFT monitoring is recommended.

3.4 HLH Considerations

This case represents an incomplete HLH phenotype (HScore 124, 9–16% probability) with a distinctive cytokine signature—IFN-γ elevation (~ 45× ULN) more prominent than IL-6—contrasting with classic HLH [6, 15]. Early hematology/critical care consultation is recommended when HLH is suspected during ICI.

3.5 Endocrine irAE

ICI-related hypophysitis with secondary adrenal insufficiency is well-recognised with anti-PD-1/PD-L1 therapy, typically 9–12 weeks after initiation [8, 11]. This case is unusual: onset at 28 weeks post-ICI—late by typical standards—and co-occurrence with a hematologic irAE and cytokine-storm biology,

suggesting the hyperinflammatory milieu may have precipitated pituitary dysfunction. Preserved mineralocorticoid axis (BP responsive to glucocorticoid alone, no hyperkalemia) supports isolated ACTH deficiency. Stress-dose steroid coverage during procedures, infections, or cytotoxic therapy is essential.

3.6 Limitations

Lack of FISH/NGS confirmation of C-MET, RB1 and TP53 immunohistochemistry not performed (canonical SCLC transformation markers; detailed in Supplementary Table S1 Methods note), GM-CSF/TPO not measured, absent bone-marrow/NK-cell data, single-patient observation, and endocrine autoantibody profiling not performed.

4. Conclusions

This is the first documented case of extreme reactive thrombocytosis (> 1,000 × 10^9/L) following ICI therapy in ES-SCLC, managed with plateletpheresis and accompanied by incomplete HLH, C-MET upregulation, and secondary adrenal insufficiency. Peak platelet count (day 71) preceding maximal tumor response (day 121) implicates immune activation as the thrombocytosis driver. C-MET upregulation (10%→80%) under PD-1 pressure represents a resistance mechanism and a targetable salvage pathway. Enhanced multi-system monitoring (platelets, CRP, IL-6, IFN-γ, ferritin, ACTH, cortisol) during the first 2–3 months of ICI therapy for ES-SCLC is recommended. Prospective studies of IL-6/GM-CSF-TPO kinetics, C-MET evolution, and multi-organ irAE clustering under ICI are warranted.

5. Lessons Learned

1. **Enhanced Platelet Monitoring**: Routine 1–2-week platelet monitoring during the first 2–3 months of ICI therapy for ES-SCLC.
2. **Therapeutic Plateletpheresis**: For PLT > 1,000 × 10^9/L with hypercoagulability or clinical thrombosis.
3. **Cytokine Storm Monitoring**: Combined CRP, IL-6, IFN-γ, ferritin, sIL-2R monitoring; marked elevations should prompt HScore.
4. **HLH Assessment**: HScore and hematology/critical care consultation for concurrent fever, hyperferritinemia (> 3,000 ng/mL), and IFN-γ elevation during ICI.
5. **C-MET-Targeted Salvage**: For SCLC with C-MET strong positivity (≥ 80%) on biopsy post-ICI, MET-targeted agents (anlotinib; tepotinib, capmatinib) are evidence-based.
6. **Adrenal Axis Surveillance**: Baseline and serial ACTH/cortisol in ICI monitoring, especially in cachectic/anorectic patients; stress-dose glucocorticoid coverage is essential during intercurrent illness.

Declarations

Ethics approval and consent to participate

All procedures performed in this study were in accordance with the ethical standards of the institutional and/or national research committee and with the 1964 Helsinki Declaration and its later amendments or comparable ethical standards. This case report was reviewed by the Ethics Committee of Hainan Cancer Hospital (Ethics Committee Reference: EC-AF-003-01.0; Approval No.: **2026□□□□40□**) and was granted exemption from full Institutional Review Board (IRB) review, on the basis that it is a retrospective case report using only previously collected, de-identified clinical data. The authors are accountable for all aspects of the work and ensure that questions related to the accuracy or integrity of any part of the work are appropriately investigated and resolved.

The requirement for informed consent was waived by the Ethics Committee of Hainan Cancer Hospital (Approval No.: **2026□□□□40□**) for this retrospective case report using only previously collected, de-identified clinical data, in accordance with the institutional policy on retrospective case reports. A copy of the ethics approval is available for review by the Editor-in-Chief of this journal on request.

Consent for publication

Written informed consent for publication of this case report and accompanying clinical data, imaging, and pathology images was waived by the Ethics Committee of Hainan Cancer Hospital (Approval No.: **2026□□□□40□**) on the basis that only de-identified retrospective clinical data were used. Identifying information has been removed in accordance with the institutional de-identification protocol.

Competing interests

All authors have completed the ICMJE uniform disclosure form (available at: https://www.icmje.org/coi_disclosure.pdf). The authors declare that they have no competing interests.

Funding

The authors received no specific funding for this work.

Authors’ contributions

C.H. and Z.Z. conceived the study. C.H. curated the clinical data, performed the formal analysis and visualization, and wrote the original manuscript draft. J.W. performed clinical investigation and provided clinical resources. X.W. performed pathology investigation and visualization. Q.C. performed clinical investigation and visualization. Z.Z. supervised the study, administered the project, acquired funding, and reviewed and edited the manuscript. All authors read and approved the final manuscript.

Acknowledgements

The authors thank the patient and his family for their consent and cooperation. The authors thank the Department of Hematology, Hainan Cancer Hospital, for hematology consultation, and the Department of Pathology for pathological review. The authors also thank the multidisciplinary team (MDT) of Hainan Cancer Hospital for clinical decision support during the patient's course.

Availability of data and materials

All de-identified clinical data supporting the findings of this case report—including laboratory values, imaging reports, pathology slides, and serial cytokine measurements—are available from the corresponding author on reasonable request, subject to approval by the Ethics Committee of Hainan Cancer Hospital. All identifying information has been removed in accordance with the institutional de-identification protocol.

Generative AI statement

During the preparation of this work, the authors used **Hermes Agent (powered by Anthropic Claude and MiniMax-M3 large language models)** in order to (i) improve language and style of the English manuscript draft, (ii) verify reference formatting and consistency, (iii) extract and review content from the ethics approval PDF and supplementary documents, and (iv) assist with compliance checking against CARE guidelines and ICMJE recommendations. After using these tools, the authors reviewed and edited the content as needed and take(s) full responsibility for the content of the publication. **No generative AI was used for study design, data collection, data analysis, interpretation of results, or drafting of scientific conclusions. All clinical data, diagnostic interpretations, and clinical recommendations are the authors' own.**

References

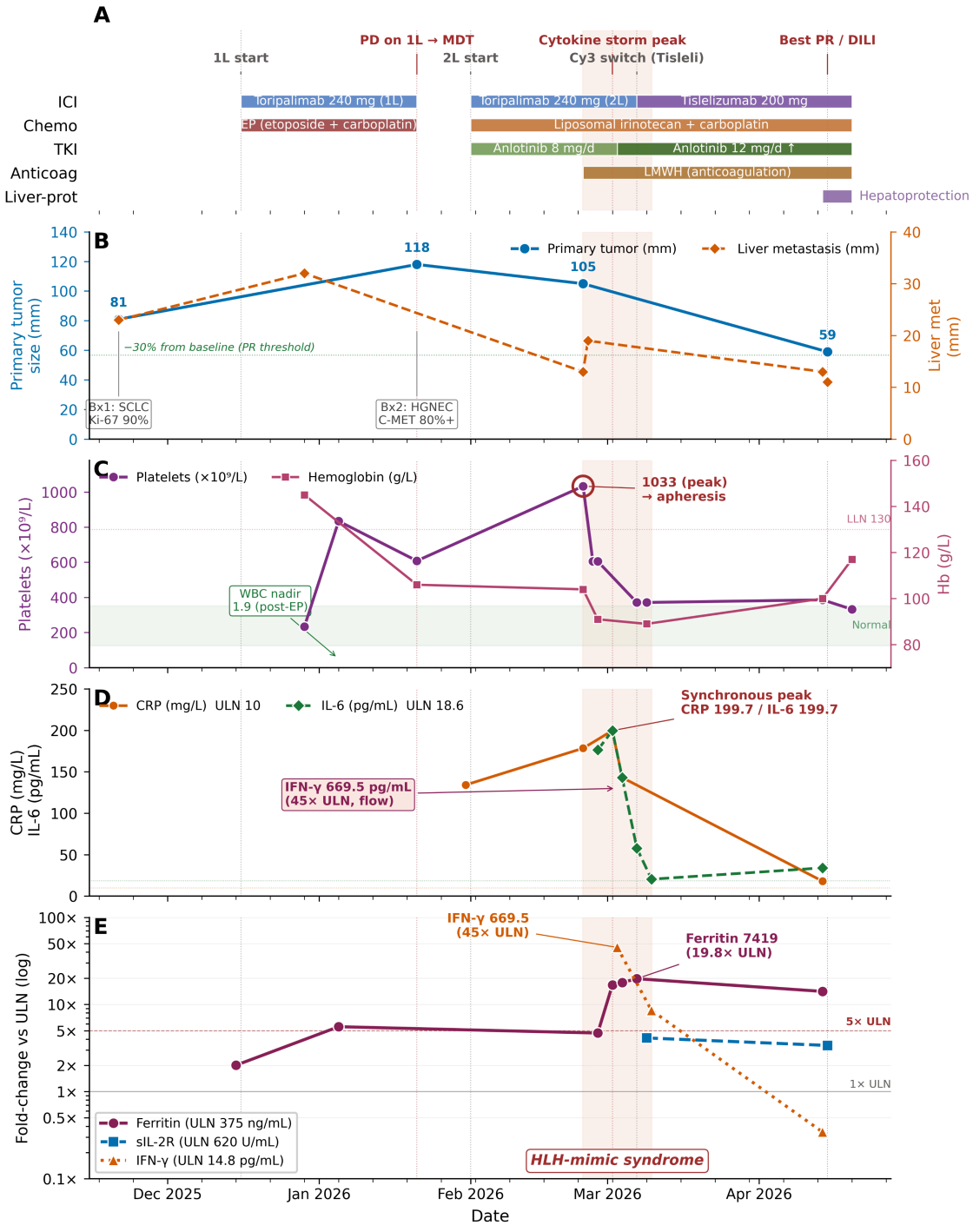
1. Michot JM, Bigenwald C, Champiat S et al. Immune-related adverse events with immune checkpoint blockade: a comprehensive review. Eur J Cancer. 2016;54:139–148. https://doi.org/10.1016/j.ejca.2015.11.016 PMID: 26765102.
2. Wang DY, Salem JE, Cohen JV et al. Fatal toxic effects associated with immune checkpoint inhibitors: a systematic review and meta-analysis. JAMA Oncol. 2018;4(12):1721–1728. https://doi.org/10.1001/jamaoncol.2018.3923 PMID: 30242316.
3. Ciurea SO, Hoffman R. Cytokines for the treatment of thrombocytopenia. Semin Hematol. 2007;44(3):166–182. https://doi.org/10.1053/j.seminhematol.2007.04.005 PMID: 17631181.
4. Shiuan E, Beckermann KE, Ozgun A et al. Thrombocytopenia in patients with melanoma receiving immune checkpoint inhibitor therapy. J Immunother Cancer. 2017;5:8.

https://doi.org/10.1186/s40425-017-0210-0 PMID: 28239462.

5. Delanoy N, Michot JM, Comont T et al. Haematological immune-related adverse events induced by anti-PD-1 or anti-PD-L1 immunotherapy: a descriptive observational study. Lancet Haematol. 2019;6(1):e48-e57. https://doi.org/10.1016/S2352-3026(18)30175-3 PMID: 30528137.
6. Liu LL, Skribek M, Harmenberg U et al. Systemic inflammatory syndromes as life-threatening side effects of immune checkpoint inhibitors: case report and literature review. J Immunother Cancer. 2023;11(3):e005841. https://doi.org/10.1136/jitc-2022-005841 PMID: 36878533.
7. He L, Zhuang Y, Zhang D et al. PD-1 blockader-associated atypical hemophagocytic lymphohistiocytosis: a cautionary case report. Transfus Apher Sci. 2023;62(2):103603. https://doi.org/10.1016/j.transci.2022.103603 PMID: 36470726.
8. Sadaat M, Jang S. Hemophagocytic lymphohistiocytosis with immunotherapy: brief review and case report. J Immunother Cancer. 2018;6(1):49. https://doi.org/10.1186/s40425-018-0365-3 PMID: 29871698.
9. Ireland AS, Micinski AM, Kastner DW et al. MYC drives temporal evolution of small cell lung cancer subtypes by reprogramming neuroendocrine fate. Cancer Cell. 2020;38(1):60–78.e12. https://doi.org/10.1016/j.ccell.2020.05.001 PMID: 32473656.
10. Boccaccio C, Comoglio PM. Invasive growth: a MET-driven genetic programme for cancer and stem cells. Nat Rev Cancer. 2006;6(8):637–45. https://doi.org/10.1038/nrc1912. PMID: 16862193.
11. Haanen JBAG, Carbonnel F, Robert C et al. Management of toxicities from immunotherapy: ESMO Clinical Practice Guidelines for diagnosis, treatment and follow-up. Ann Oncol. 2018;29 Suppl 4:iv264-iv266. https://doi.org/10.1093/annonc/mdy162 PMID: 29917046.
12. Thompson JA, Schneider BJ, Brahmer J et al. NCCN Guidelines® Insights: management of immunotherapy-related toxicities, version 2.2024. J Natl Compr Canc Netw. 2024;22(9):582–592. https://doi.org/10.6004/jnccn.2024.0057 PMID: 39536465.
13. Paik PK, Felip E, Veillon R et al. Tepotinib in non-small-cell lung cancer harboring MET exon 14 skipping. N Engl J Med. 2020;383(10):931–943. https://doi.org/10.1056/NEJMoa2004407 PMID: 32469185.
14. Wolf J, Seto T, Han JY et al. Capmatinib in MET exon 14-mutated or MET-amplified non-small cell lung cancer. N Engl J Med. 2020;383(10):944–957. https://doi.org/10.1056/NEJMoa2002787 PMID: 32877583.
15. Walmsley CS, Schoepflin Z, De Brabandt C et al. Hemophagocytic lymphohistiocytosis associated with immune checkpoint inhibitor use: a review of the current knowledge and future directions. Blood Cells Mol Dis. 2025;110:102896. https://doi.org/10.1016/j.bcmd.2024.102896 PMID: 39366077.
16. Cheng Y, Wang Q, Li K, et al. Anlotinib vs placebo as third- or further-line treatment for patients with small cell lung cancer: a randomised, double-blind, placebo-controlled phase 2 study (ALTER1202). Br J Cancer. 2021;125(3):366–71. https://doi.org/10.1038/s41416-021-01356-3. PMID: 34006926 (ClinicalTrials.gov: NCT02388919).

17. Zhang L, Geng Z, Hao B et al. Tislelizumab: a modified anti-tumor programmed death receptor 1 (PD-1) antibody with reduced binding to FcγR. Cancer Control. 2022;29:10732748221111296. https://doi.org/10.1177/10732748221111296 PMID: 35926155.
18. Gu Y, Benavente CA. Landscape and treatment options of shapeshifting small cell lung cancer. J Clin Med. 2024;13(11):3120. https://doi.org/10.3390/jcm13113120 PMID: 38892831.
19. Paz-Ares L, Dvorkin M, Chen Y, et al. Durvalumab plus platinum-etoposide versus platinum-etoposide alone in first-line treatment of extensive-stage SCLC (CASPIAN): a randomised, controlled, open-label, phase 3 trial. Lancet. 2019;394(10212):1929–39. https://doi.org/10.1016/S0140-6736(19)32222-6. PMID: 31590988 (ClinicalTrials.gov: NCT03043872).
20. Horn L, Mansfield AS, Szczęsna A, et al. First-line atezolizumab plus chemotherapy in extensive-stage small-cell lung cancer. N Engl J Med. 2018;379(23):2220–9. https://doi.org/10.1056/NEJMoa1809064. PMID: 30280641 (ClinicalTrials.gov: NCT02763579).
21. Cheng Y, Han L, Wu L, et al. Effect of first-line serplulimab versus placebo added to chemotherapy on survival in extensive-stage small-cell lung cancer (ASTRUM-005): a phase 3, international, randomised, double-blind, placebo-controlled study. JAMA. 2022;328(12):1223–32. https://doi.org/10.1001/jama.2022.16464. PMID: 36166026 (ClinicalTrials.gov: NCT04060392).
22. Wang J, Zhou C, Yao W, et al. Adebrelimab or placebo plus carboplatin and etoposide as first-line treatment for extensive-stage small cell lung cancer (CAPSTONE-1): a phase 3, randomised, double-blind, placebo-controlled, phase 3 trial. Lancet Oncol. 2022;23(6):739–47. https://doi.org/10.1016/S1470-2045(. 22)00224-8 PMID: 35576956 (ClinicalTrials.gov: NCT03703297).
23. Fardet L, Galicier L, Lambotte O et al. Development and validation of the HScore, a score for the diagnosis of reactive hemophagocytic syndrome. Arthritis Rheumatol. 2014;66(9):2613–2620. https://doi.org/10.1002/art.38690 PMID: 24782338.
24. Gagnier JJ, Kienle G, Altman DG et al. The CARE guidelines: consensus-based clinical case reporting guideline development. BMJ Case Rep. 2013. https://doi.org/10.1136/bcr-2013-201554 PMID: 24155002.
25. Kaser A, Brandacher G, Steurer W et al. Interleukin-6 stimulates thrombopoiesis through thrombopoietin: role in inflammatory thrombocytosis. Blood. 2001;98(9):2720–2725. https://doi.org/10.1182/blood.V98.9.2720 PMID: 11675343.

Figures



Shaded coral band = "cytokine-storm window" (Feb 24 – Mar 10, 2026). Vertical dotted lines mark major treatment / clinical events.

Figure 1

Comprehensive clinical course of a 62-year-old man with ES-SCLC transforming to HG-NEC (C-MET 80%+), complicated by PD-1 inhibitor-related cytokine activation, HLH-mimic syndrome, and secondary adrenal insufficiency. All panels share a common time axis spanning December 2025 to June 2026; the coral band marks the cytokine-storm window (24 February–10 March 2026). (A) Treatment timeline: sequential ICI (Toripalimab 240 mg in first and second line, switched to Tislelizumab 200 mg from the

third cycle), platinum-based chemotherapy (etoposide+carboplatin first line, liposomal irinotecan+carboplatin second line), anlotinib 8→12 mg/d escalation (3 March 2026), low-molecular-weight heparin (LMWH) anticoagulation, hepatoprotective therapy, and consolidative thoracic radiotherapy commencing 23 May 2026. (B) Tumor burden: primary lung mass longest diameter (blue, left axis) decreased from 118 mm (2025-11-21 baseline) to 59 mm (2026-04-15 PR), and hepatic metastasis (orange, right axis) from 23 mm (2025-11-21 PET/CT baseline) to 11 mm (2026-04-15 CT)—both exceeding the −30% RECIST 1.1 partial-response threshold. Biopsy timings are annotated (Bx1: right supraclavicular lymph node, November 2025; Bx2: right lung mass, January 2026). (C) Hematologic dynamics: platelets peaked at 1,033 × 10^9/L (24 February 2026, apheresis indicated, red ring), then normalized; hemoglobin declined to a nadir of 89 g/L; WBC nadir of 1.9 × 10^9/L following etoposide-platinum is annotated. (D) Acute inflammatory markers: CRP (orange, ULN 10 mg/L) and IL-6 (green, ULN 18.6 pg/mL) peaked synchronously on 2 March 2026 at 199.7 mg/L and 199.7 pg/mL, respectively; intracellular IFN-γ flow cytometry surged to 669.5 pg/mL (~45× ULN). (E) HLH-mimic biomarker triad on a logarithmic fold-change scale versus ULN: ferritin reached 7,419 ng/mL (19.8× ULN, magenta), sIL-2R reached 2,562 U/mL (4.1× ULN, blue), and IFN-γ reached 669.5 pg/mL (45× ULN, orange)—all three crossing the 5× ULN sentinel threshold.

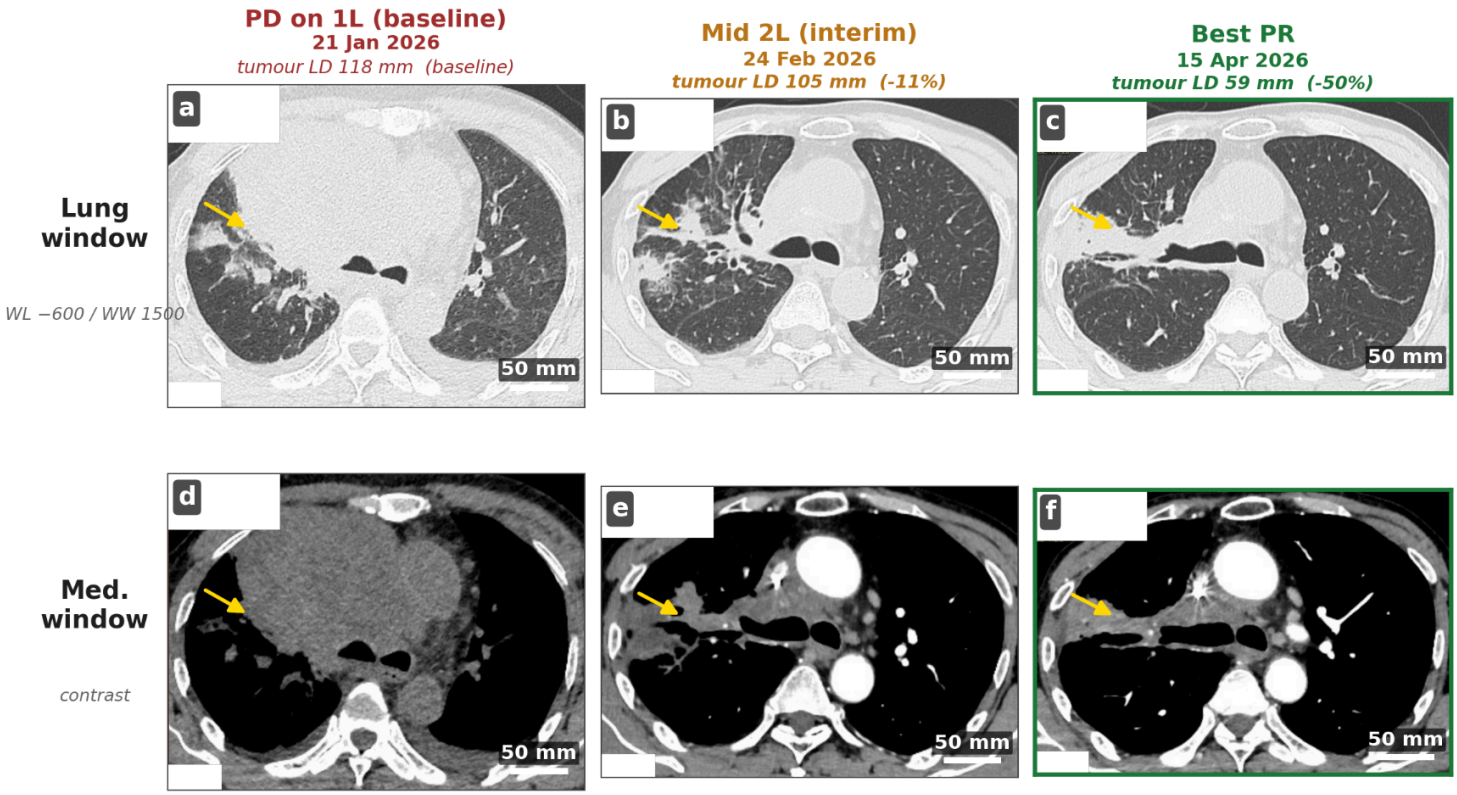


Figure 2

Serial contrast-enhanced axial CT at the carinal level demonstrating radiologic response of the right-lung primary mass to sequential immunochemotherapy plus anlotinib. Three time points are shown in lung-window (top row, a–c) and contrast-enhanced mediastinal-window (bottom row, d–f) reconstructions: (A,

D) 21 January 2026 (baseline before second-line therapy, tumor longest diameter 118 mm); (B, E) 24 February 2026 (after two cycles of second-line therapy, 11% early shrinkage); (C, F) 15 April 2026 (continued response, tumor longest diameter 59 mm, 50% reduction; partial response per RECIST 1.1). All images are at the same anatomical level to allow direct slice-by-slice comparison. Note that the carinal plane shown does not represent the maximum cross-section of the tumor; whole-tumor longest diameters are reported in Figure 1B.

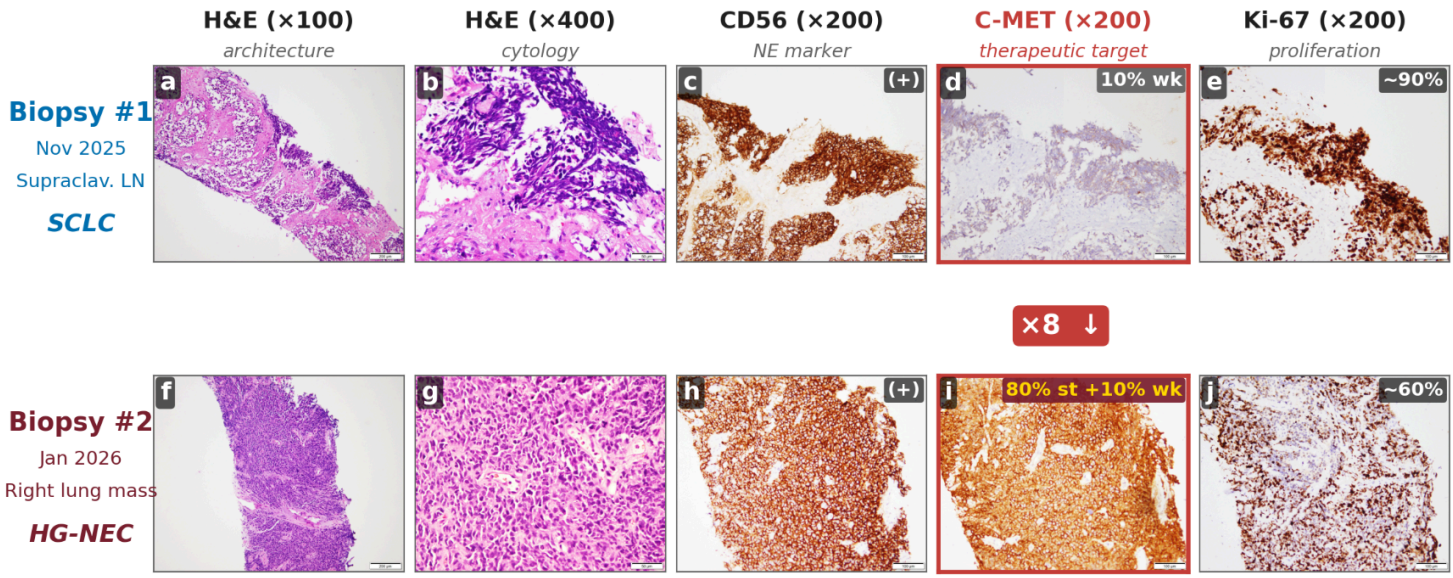


Figure 3

Comparative histology and immunohistochemistry of sequential biopsies documenting pathological transformation from SCLC to HG-NEC. (a, b) Biopsy #1 (November 2025; right supraclavicular lymph node): small round-blue cells with nuclear molding, scant cytoplasm, and crush artifact, consistent with classical SCLC. (c) Strong diffuse CD56 membrane expression confirming neuroendocrine differentiation. (d) C-MET immunostaining showing only sparse weak cytoplasmic staining (~10% of tumor cells, weak intensity). (e) Ki-67 nuclear labeling index >90%, consistent with high-grade SCLC. (f, g) Biopsy #2 (January 2026; right lung mass): solid sheets of larger polygonal cells with vesicular nuclei and prominent nucleoli, reduced crush artifact, consistent with HG-NEC transformation. (h) C-MET showing strong diffuse membrane staining in 80% of tumor cells with additional 10% weak-positive component. Scale bars = 100 μm.

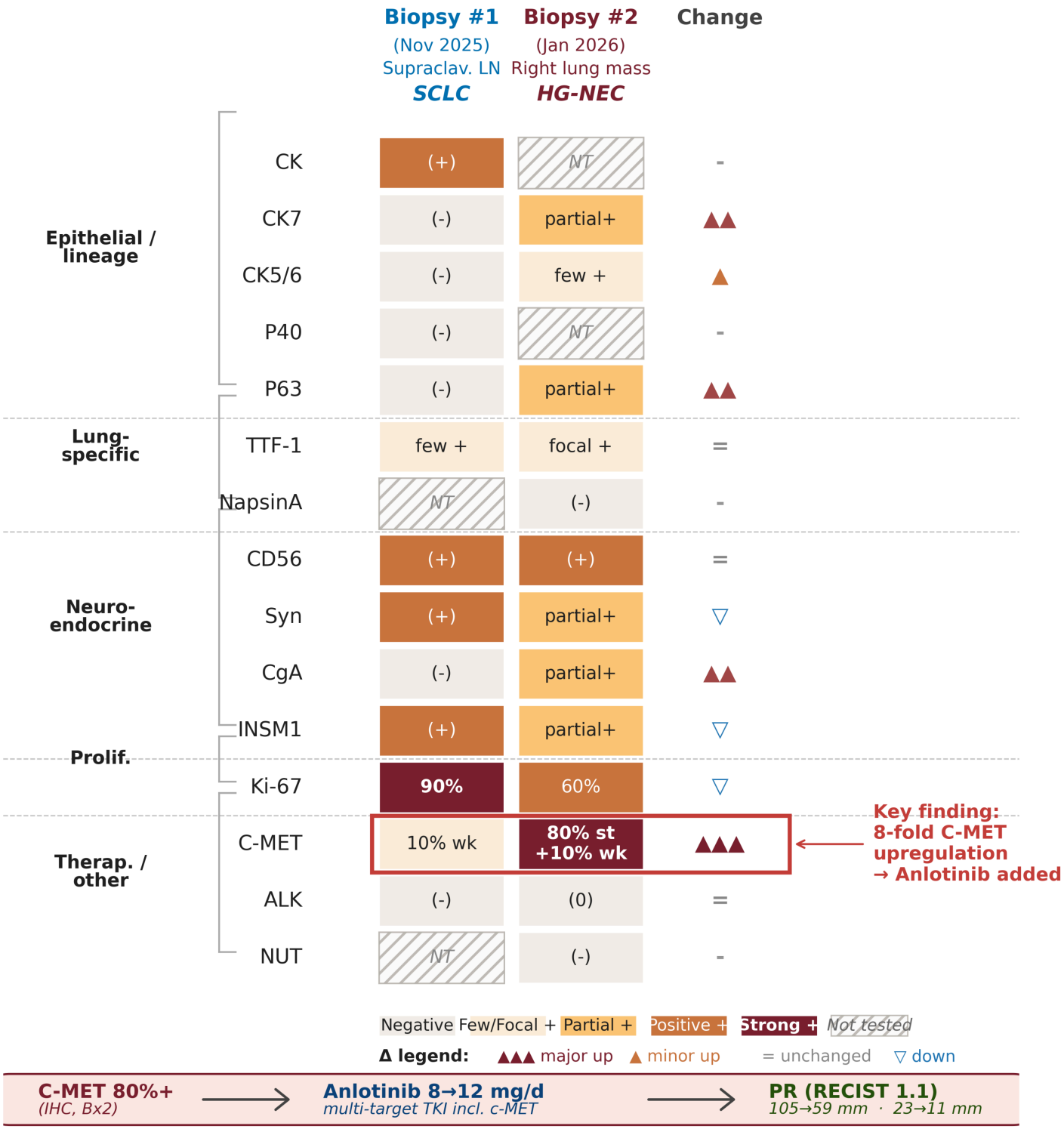


Figure 4

Comparative IHC marker panel heatmap across 15 markers for Biopsy #1 (right supraclavicular lymph node, November 2025; SCLC) and Biopsy #2 (right lung mass, January 2026; HG-NEC). Markers are organised by biological function: epithelial/lineage (CK, CK7, CK5/6, P40, P63), lung-specific (TTF-1, NapsinA), neuroendocrine (CD56, Syn, CgA, INSM1), proliferation (Ki-67), and therapeutic targets (C-MET, ALK, NUT). Each cell is colour-coded on a five-level discrete IHC scale (Negative, Few/Focal +, Partial +,

Positive +, Strong +); hatched fill indicates markers not assessed. The right-hand annotations indicate the therapeutic relevance of C-MET upregulation and the shift in neuroendocrine marker profile (Syn and INSM1 partial attenuation, CgA newly acquired).

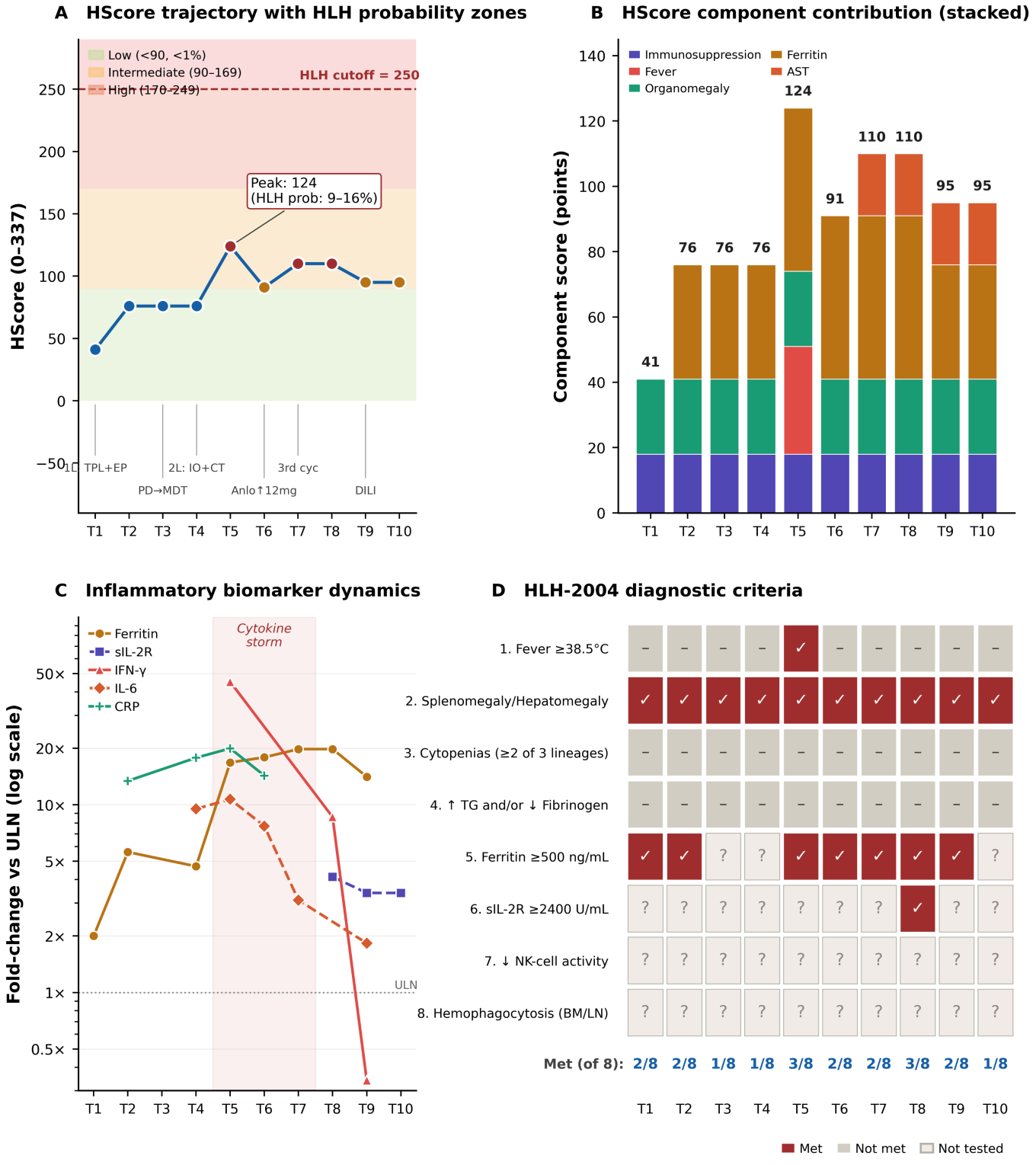


Figure 5

Dynamic HScore trajectory and HLH-mimic syndrome evolution. (A) HScore trajectory across 10 timepoints (T1–T10, December 2025–April 2026). The HScore rose from 41 at baseline to a peak of 124 at T5 (2026-03-02, corresponding to peak HLH-mimic activity and IL-6 surge), falling within the intermediate-probability zone (9–16% HLH probability). Treatment milestones are annotated: 1L, first-line Toripalimab+EP; PD→MDT, disease progression and multidisciplinary team review; 2L, second-line IO+chemotherapy; Anlo↑12 mg, Anlotinib dose escalation to 12 mg/d; TPL, therapeutic plateletpheresis; DILI, drug-induced liver injury. The dashed red line marks the HLH diagnostic cutoff (HScore 250). (B) Stacked component contributions to the HScore at each timepoint. Immunosuppression (sIL-2R) and organomegaly contributed throughout; ferritin elevation appeared at T2 and peaked at T5; fever and AST elevation contributed at later timepoints. (C) Inflammatory biomarker dynamics expressed as fold-change relative to the upper limit of normal (ULN, log scale). IFN-γ (red) peaked at ~45× ULN at T5 before declining rapidly; ferritin (gold) rose progressively to ~20× ULN between T7–T8; IL-6, CRP, and sIL-2R remained elevated above ULN during the cytokine storm window (shaded pink, T5–T7). (D) HLH-2004 diagnostic criteria heatmap (✓ = criterion met; – = not met; ? = not tested). At peak (T5), only three of eight criteria were met (splenomegaly/hepatomegaly, ferritin ≥500 ng/mL, fever ≥38.5°C), below the diagnostic threshold of five of eight. Criteria 5 (TG/fibrinogen) and 6 (sIL-2R ≥2,400 U/mL) were not met at any timepoint; NK-cell activity (criterion 7) and bone marrow hemophagocytosis (criterion 8) were not tested.

Supplementary Files

This is a list of supplementary files associated with this preprint. Click to download.

- TableS1IHCMarkerPanel.docx